Metallomics

Integrated biometal science

www.rsc.org/metallomics

Volume 5 | Number 8 | August 2013 | Pages 939–1078

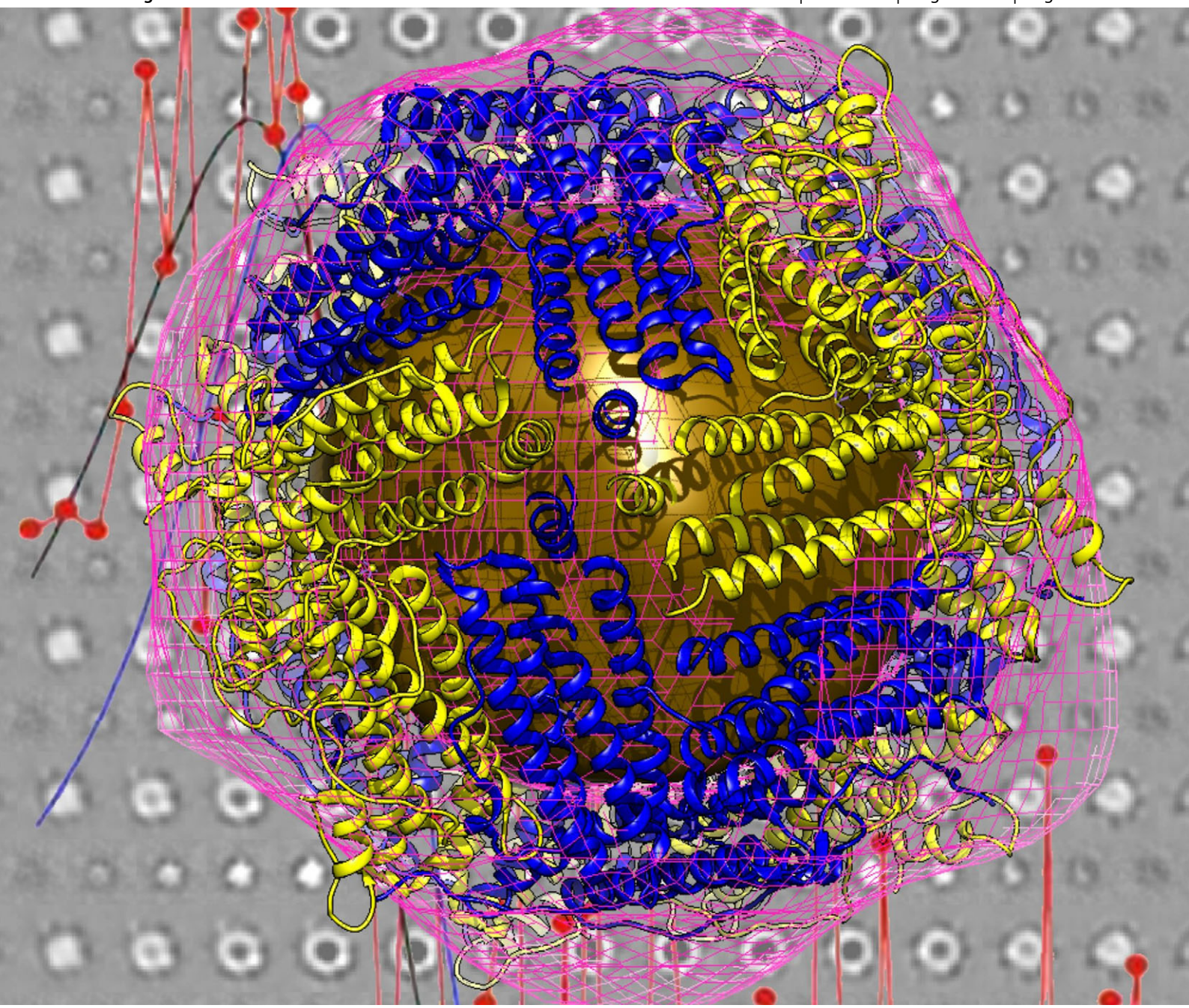

ISSN 1756-5901

RSC Publishing

PAPER

Fanis Missirlis *et al*.
Biophysical and genetic analysis of iron partitioning and ferritin function in *Drosophila melanogaster*

Indexed in MEDLINE!

1756-5901(2013)5:8;1-Z

Metallomics

RSC Publishing

PAPER

Biophysical and genetic analysis of iron partitioning and ferritin function in *Drosophila melanogaster*†

Cite this: *Metallomics*, 2013, **5**, 997

Lucía Gutiérrez,‡[a] Kristina Zubow,‡[b] Jon Nield,‡[b] Alexis Gambis,[c] Bertrand Mollereau,[d] Francisco J. Lázaro[e] and Fanis Missirlis*[f]

Received 11th April 2013,
Accepted 5th June 2013

DOI: 10.1039/c3mt00118k

www.rsc.org/metallomics

Metals have vital functions as prosthetic groups in enzymes, but in labile form they can propagate oxidative stress. The primary function of ferritin is to store bioavailable iron in the form of ferrihydrite. In animals, ferritin is also used to traffic and recycle iron, and to modulate intestinal iron absorption. However, the effect of ferritin accumulation on cellular iron bioavailability remains poorly understood. Moreover, putative *in vivo* interactions of ferritin with other metal ions have been proposed, but their physiological relevance remains unclear. Here, heterozygous mutant and overexpression ferritin strains of *Drosophila melanogaster* were subjected to dietary iron manipulations to study the dynamics of iron partition between ferritin and other proteins. Quantitative magnetic analysis of whole fly samples indicated that iron loading of the ferritin core varied in the different genotypes. Total paramagnetic iron content, a likely correlate of bioavailable iron, was reduced in flies overexpressing ferritin when compared with control *white* flies. Further, three-dimensional maps of the ferritin protein shell and iron core were obtained from single particle transmission electron microscopy imaging and confirmed the similarity between *Drosophila* and *Trichoplusia* ferritin structures. Purified *Drosophila* ferritin also contained small amounts of zinc and manganese. Flies that overexpressed ferritin accumulated in their bodies half the amount of manganese compared to their respective controls. Our results indicate that ferritin may be involved in the homeostasis of other divalent metals, besides iron, and that overexpression of ferritin, sometimes employed to rescue neurodegenerative models of disease, serves to limit divalent metal bio-availability in cells.

Introduction

Ferritin is an iron storage protein complex whose function is conserved in evolution.[1–4] It has been used as a probe in magnetic resonance imaging (MRI)[5–8] and for the delivery of pharmaceuticals or other small molecules to specific cells.[9–12] In rodents, ferritin overexpression protects against acute paradigms of chemically induced neuronal degeneration[13] and liver ischemia reperfusion injury,[14] but is also associated with neurodegeneration[15] and lymphoma[16] when overexpression is prolonged. It has been suggested that ferritin overexpression causes the sequestering of otherwise bioavailable iron thereby depleting functional iron in cells,[17] however no direct measurements of the labile iron pool have been performed in ferritin overexpression systems due to the difficulty of distinguishing different forms of iron *in vivo*. Concentration and chemical speciation of iron in biological matter can be assessed by magnetic characterisation. Among different magnetism-based techniques, alternating current (AC) susceptibility is especially suitable to discern between ferritin iron (iron in the form of inorganic crystallites at the core of the ferritin protein that show superparamagnetism at high temperature and magnetic relaxation below the so-called blocking temperature) and paramagnetic iron (nonmineralised iron usually in the form of

[a] *Instituto de Ciencia de Materiales de Madrid, ICMM-CSIC, Cantoblanco, Madrid, 28049, Spain. E-mail: lucia@icmm.csic.es*
[b] *School of Biological and Chemical Sciences, Queen Mary University of London, Mile End Road, London, E1 4NS, UK. E-mail: k.zubow@qmul.ac.uk, j.nield@qmul.ac.uk*
[c] *Howard Hughes Medical Institute, Laboratory of Apoptosis and Cancer, The Rockefeller University, New York, NY 10065, USA. E-mail: agambis@gmail.com*
[d] *Laboratory of Molecular Biology of the Cell, UMR5239 CNRS/Ecole Normale Supérieure de Lyon, IFR 128 Biosciences Lyon Gerland, Université de Lyon, Lyon, France. E-mail: Bertrand.Mollereau@ens-lyon.fr*
[e] *Departamento de Ciencia y Tecnología de Materiales y Fluidos, Universidad de Zaragoza, Zaragoza, 50018, Spain. E-mail: osoro@unizar.es*
[f] *Departamento de Fisiología, Biofísica y Neurociencias, Centro de Investigación y de Estudios Avanzados, Av. IPN 2508, CP 07360, Mexico City, Mexico. E-mail: fanis@fisio.cinvestav.mx*

† Electronic supplementary information (ESI) available. See DOI: 10.1039/c3mt00118k

‡ Equal contributing authors.

various organic molecules).[18] Other iron containing species may exist in biological media but either due to their negligible magnetism or to their very low concentration it is still feasible to use the above mentioned technique to obtain speciation-dependent, information, of much help, for example, in studies of iron-containing drug metabolism and genetic iron-related disorders.[18,19] Here, we sought to expose newly developed technologies to *Drosophila melanogaster* flies that overexpress ferritin.[20,21]

Drosophila makes two types of ferritin; the testis-specific mitochondrial protein encoded by the X-chromosome *Ferritin 3 Heavy Chain Homologue* (*Fer3HCH*) gene[22] and the major secretory type (hereby referred to as *Drosophila* ferritin) responsible for systemic iron storage.[20,23–25] Radioactive tracing showed that most ingested iron accumulates in *Drosophila* ferritin,[20,22] the product of Fer1HCH and Fer2LCH, which provide for the ferroxidase activity and the iron nucleation sites required for mineralization of the ferrihydrite iron core.[26–28] Iron-loaded ferritin was recently shown to promote cell proliferation.[29] Genetic alterations in the expression of ferritin had negligible effects in the amount of total iron associated with ferritin,[20] suggesting that additional aspects to the regulation of ferritin protein synthesis and degradation determine ferritin iron loading. The present investigation was undertaken to test whether ferritin overexpression affected bioavailable iron, given the reported protective role of neuronal ferritin overexpression in *Drosophila* models of disease attributed to ferritin's iron-sequestering antioxidant function.[30–33]

Moreover, the relationship of ferritin with other divalent metals than iron remains poorly understood. Interestingly, Metal Transcription Factor-1 (MTF-1) regulates ferritin in response to dietary zinc treatment.[34,35] Ferritin induction by iron (seen in the anterior midgut) proceeds normally in MTF-1 mutants, whereas zinc specifically induces ferritin in the posterior midgut *via* MTF-1.[35] MTF-1 binding sites are conserved in the ferritin locus of many *Drosophila* species,[20,36] but the biological relevance of this interaction remains obscure. Ferritin can bind up to 6 atoms of zinc per molecule of holoferritin in rabbits[37] and human serum ferritin was also recently shown to bind zinc.[38] Ferritin binding sites for zinc have likely been ignored by workers in the field given that more than 1000 atoms of iron are normally mineralized in isolated holoferritin and because processes similar to metal core reconstitution[39–42] are not likely to occur *in vivo*. Here, the binding of other metals to *Drosophila* ferritin as purified from flies fed on iron was examined, along with the effects on metal accumulation in the bodies of flies overexpressing ferritin in comparison to control flies.

Materials and methods

Drosophila cultures

Flies were kept at 25 °C under 12 hour light dark cycles and were grown on a standard medium, or with 1 mM ferric ammonium citrate (FAC) to generate an iron overload or 200 μM bathophenanthroline sulfate (BPS) to generate an iron deficiency.[22,24] Strain *Fer1HCH*^{G188}/*TM3*, *Kr-GFP*, *Ser* encodes a GFP fused to Fer1HCH *in vivo* and has been characterized elsewhere.[20] Ferritin overexpression using *Actin-Gal4*/+; *UAS-Fer1HCH*, *UAS-Fer2LCH*/+ flies has also been used and described previously.[20,21,25,32] Strain *Df(3R)Fer*/*TM3*, *Kr-GFP*, Ser creates a 2.2 kb deletion (confirmed by Southern Blot) removing parts of the open reading frame of both ferritin subunits.

Ferritin isolation

We followed a slightly modified procedure previously used to isolate mosquito ferritin.[43] Iron-fed flies (12 g) were collected in liquid nitrogen and pulverised in a mortar under liquid nitrogen. The disrupted flies were suspended in 5 mM phenylthiourea, 50 mM HEPES pH 7.5 and sonicated for 5 × 45 s at 55% maximum power on Sonics, Vibra Cell on ice. The suspension was then centrifuged at 15 000 × *g* for 15 min at 4 °C and the supernatant was filtered through four layers of filter paper (Whatman). The filtrate was submitted to ultracentrifugation at 180 000 × *g* (Beckman 90 Ti rotor) for 1 hour at 15 °C. The resulting pellet contained ferritin and was further resuspended in 50 mM HEPES pH 7.5 and incubated at 75 °C for 15 min following a centrifugation at 15 000 × *g* for 15 min at 4 °C. A final ultracentrifugation in a saturated KBr solution at 180 000 × *g* for 22 hours at 15 °C resulted in a sample of ferritin purified away from other proteins (Fig. 1B). The pellet was collected in 50 mM HEPES pH 7.5 and residues of KBr were removed by ultrafiltration using Viovaspin 500 (10 kDa MWCO) columns.

Elemental analysis

Purified ferritin or whole flies were freeze-dried, weighed and acid digested for the elemental analysis using a 4 : 1 (v/v) 65% HNO_3 (w/v) and 30% H_2O_2 (w/v) solution and microwave

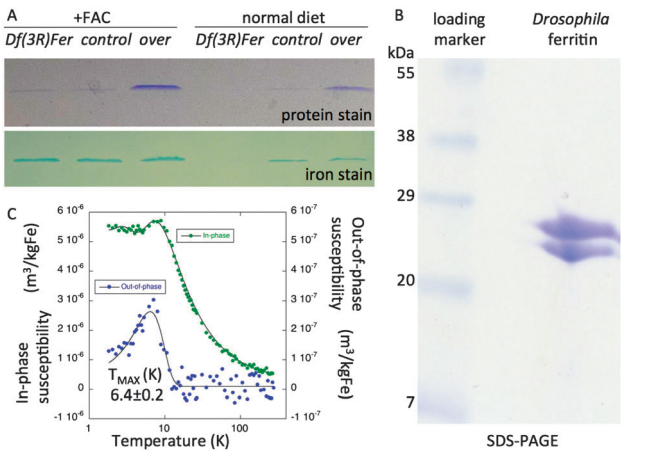

Fig. 1 Genotype and diet effects on the iron loading of ferritin. (A) Representative SDS-PAGE analysis (non-denaturing conditions) from whole-fly protein samples from *Df(3R)Fer*/+ heterozygotes (*Df(3R)Fer*), *white* controls (*control*) and *Actin-Gal4*/+; *UAS-Fer1HCH*, *UAS-Fer2LCH*/+ ferritin overexpressors (*over*) grown with (first 3 lanes) and without (lanes 4–6) 1 mM FAC addition to the diet. Top gel was stained with Coomassie blue to reveal protein, whereas lower gel was stained with Prussian blue to reveal iron. (B) SDS-PAGE analysis (denaturing conditions) of the isolated ferritin revealed by Coomassie Brilliant Blue. Fer2LCH corresponds to the 27 kDa band and Fer1HCH to the 25 kDa band. (C) Temperature dependence of the in-phase and out-of-phase AC magnetic susceptibilities of purified *Drosophila* ferritin. Note the out-of-phase T_{MAX} for purified ferritin at 6.4 ± 0.2 K and the corresponding shoulder appearing for the in-phase component.

heating. Inductively Coupled Plasma Atomic Emission Spectroscopy (ICP-AES) in a Thermo Elemental IRIS Intrepid spectrometer was used for elemental analysis of the samples.

Transmission electron microscopy

A JEOL 1230 transmission electron microscope (The NanoVision Centre, Queen Mary, University of London, UK) was used at an accelerating voltage of 80 keV in combination with a Morada 2k CCD camera (Olympus Soft Imaging Solutions, Ltd, Singapore) operating in 2048 × 2048 pixel imaging mode. To optimise the imaging conditions in terms of defocus and astigmatism, a MORADA Video Systems' fast FFT processor was used to observe the first minima of the power spectrum and place it within a range of 15 Å to 17 Å. Unstained holoferritin samples were imaged at a calibrated magnification of 80 000× followed by aliquots negatively stained with 1% uranyl acetate, the latter recorded at a magnification of 60 000×.

Image processing

A total of 28 CCD images, for unstained holoferritin, and 12 CCD images, for negatively stained holoferritin, that displayed minimal astigmatism and drift were recorded with a pixel size at the specimen level corresponding to 5.962 Å per pixel (80 000×) or 7.969 Å (60 000×), respectively. Particles were floated out into boxes using the 'boxer' command of EMAN2.[44] All subsequent image processing was performed within the Imagic-V software (Imagic Science, GmbH, Berlin, Germany) environment,[45] running *via* Mandriva Linux on a Beowulf computer cluster. A data set of 4170 unstained and 20 341 negatively stained single particle images were obtained by picking all discernible single particles present. An analysis of the data sets was made starting with the reference free alignment-by-classification procedure.[46] This identified several sub-populations of particles differing in size and shape. Each sub-population was in turn analysed as a separate data set, with the reference free alignment giving the initial class averages necessary for multi-reference alignment, leading to 413 and 1874 class averages respectively with an enhanced signal-to-noise ratio. Relative orientations were determined for the class averages by the angular reconstitution technique[47] and initial 3D reconstructions gained from implementation of the exact back projection technique.[48] Reprojections were taken from each 3D model and used to identify additional atypical views and further refine the class averages within each sub-population data set. At each stage, roughly 3.5 to 5% of the class averages were discarded after assessment using cross correlation functions. Through this iterative refinement the data converged to give the best 3D reconstructions shown. Resolution was determined by calculating the Fourier Shell Correlation at both the 0.5 and 3 σ criterion between two independent 3D reconstructions.[49] The crystallographic atom co-ordinate data of the tiger moth *Trichoplusia ni* apoferritin (pdb code 1Z6O)[28] was modelled into molecular maps derived from the iron core and protein shell using PyMol (The PyMOL Molecular Graphics System, Version 1.1r1, Schrödinger, LLC) and Chimera modelling software packages.[50] Surface rendered views are shown with a threshold of 2.5 σ.

Magnetic susceptibility measurements and iron quantification procedure

The magnetic characterisation of freeze-dried whole flies (≈100 mg dry weight) and purified ferritin, previously placed in gelatine capsules, was carried out in Quantum Design MPMS-XL and MPMS-5S magnetometers equipped with an AC option, in the temperature range 1.8–300 K, at a frequency of 1 Hz and with field amplitude of 0.45 mT. The magnetic data considered in this paper are $\chi'(T)$ and $\chi''(T)$, that is, the temperature (T) dependent profiles of the in-phase and out-of-phase components of the AC magnetic susceptibility, respectively. The out-of-phase component $\chi''(T)$ is only sensitive to mineralised iron, in particular to the magnetic relaxation of ferritin below its blocking temperature, and is neatly observed when measured for a sample of purified ferritin. The presence of ferritin iron, therefore, can be assessed in biological matter by analysing this component with virtually no interferences from other iron forms. The in-phase component $\chi'(T)$ responds from both the presence of superparamagnetic ferritin and paramagnetic iron. Obtaining the ferritin iron content from the $\chi''(T)$ data allows subtraction of its contribution to $\chi'(T)$ yielding an estimation of the paramagnetic iron. The first step in quantification is to get mathematical functions $\chi'_{\text{ferritin}}(T)$ and $\chi''_{\text{ferritin}}(T)$ to fit the experimental (in-phase and out-of-phase, respectively) magnetic susceptibility data of the standard, that in our case is *Drosophila* purified ferritin. In Fig. 1C the experimental data points together with the fitting curves (continuous lines) are shown. For both components analytical functions coherent with the expected magnetic behaviour of a mixture of magnetic nanoparticles have been employed.[51] The calculations proceed by fitting (Levenberg–Marquardt algorithm) a multiple of $\chi''_{\text{ferritin}}(T)$ to the experimental $\chi''(T)$ data, the multiplicative factor a being the ferritin iron content. This is done first because of the sole dependence of $\chi''(T)$ on ferritin-type iron. Finally, a function of the type

$$a\chi'_{\text{ferritin}}(T) + c/T + d$$

is fitted with the same method to the experimental $\chi'(T)$ data, being c/T the magnetic susceptibility of the unit mass of Fe (assumed a magnetic moment of 5 μB per iron ion), d all the temperature independent contributions and yielding c as the paramagnetic iron content. The calculated error was less than 0.001 mg g^{-1} Fe for all paramagnetic iron measurements (and was therefore omitted from Table 1).

Results

Genetic manipulations of *Drosophila* ferritin

The adjacent location of Fer1HCH and Fer2LCH on the right arm of the third chromosome[52] was used to generate a small 2.2 kb deficiency that deleted their respective promoters and part of the primary transcript for both genes. Heterozygous flies for this deficiency, termed *Df(3R)Fer*, are expected to maintain a wild type expression pattern with a reduced amount of ferritin mRNA transcripts due to the halving of the DNA template.

Table 1 ICP-AES determination of metal composition of *Drosophila* strains per diet treatment as explained in the main text. Paramagnetic and ferritin iron were determined independently by analysing the temperature-dependence of AC magnetic susceptibility. Elemental concentrations in the different forms are expressed in mg per g of whole fly dry sample

Genotype	Food	[Fe] ICP-AES	[Fe] ferritin	[Fe] param.	[Cu]	[Zn]	[Mn]
Df(3R)Fer	BPS	0.136	0.14 ± 0.05	0.066	0.019	0.074	0.036
Fer1HCH^{G188}	BPS	0.170	0.18 ± 0.08	0.055	0.022	0.079	0.029
Control	BPS	0.193	0.08 ± 0.07	0.062	0.018	0.076	0.040
Over	BPS	0.154	0.04 ± 0.04	0.047	0.016	0.072	0.021
Df(3R)Fer	Normal	0.202	0.08 ± 0.07	0.070	0.021	0.083	0.038
Fer1HCH^{G188}	Normal	0.191	0.10 ± 0.06	0.061	0.020	0.072	0.033
Control	Normal	0.292	0.21 ± 0.07	0.075	0.019	0.087	0.035
Over	Normal	0.203	0.14 ± 0.05	0.039	0.017	0.075	0.023
Df(3R)Fer	FAC	0.554	0.57 ± 0.06	0.078	0.021	0.077	0.037
Fer1HCH^{G188}	FAC	0.678	0.86 ± 0.08	0.115	0.024	0.077	0.033
Control	FAC	0.735	0.60 ± 0.07	0.130	0.018	0.078	0.039
Over	FAC	0.438	0.57 ± 0.05	0.062	0.016	0.072	0.021

These flies were used to investigate the effects of producing less ferritin under previously established dietary conditions of iron limitation, sufficiency and excess.[22,24] Conversely, the inducible *UAS-Fer1HCH, UAS-Fer2LCH* transgenes driven by the ubiquitous *Actin-Gal4* were used to overexpress ferritin in most cell types.[20,21,25,32] Coomassie blue stain following SDS-PAGE of whole fly lysates revealed ferritin as the major high molecular weight protein, while Prussian blue stain revealed the iron it contains.[20,22,53] Flies grown on 1 mM FAC contained approximately similar amounts of iron in their ferritins, despite differences in protein amounts (Fig. 1A and Fig. S1, ESI†). In contrast, under normal diet, less iron was stored in *Df(3R)Fer* heterozygotes compared to the white strain, which we used as a control. *Actin-Gal4*/+; *UAS-Fer1HCH*, *UAS-Fer2LCH*/+ flies (termed here *over* flies for ubiquitous ferritin overexpression) did not accumulate excess iron in either dietary condition, despite making more protein (Fig. 1A), suggesting less iron was loaded to ferritin (either on average or some ferritin shells remained relatively iron-poor) in this genotype.

Magnetic characterization and elemental analysis of *Drosophila* ferritin

Drosophila ferritin was purified adapting the method described by Dunkov *et al.* to isolate mosquito ferritin.[43] Biochemical isolation relied on the thermal stability of the assembled ferritin complex and its high density due to the iron core. Purity of the sample was determined by SDS-PAGE, which revealed both ferritin subunits in similar amounts (Fig. 1B). The temperature dependence of the AC magnetic susceptibility of the pure fly ferritin had two discrete components: in-phase susceptibility (χ') showed a shoulder at around 10 K that together with the out-of-phase susceptibility (χ'') maximum observed at slightly lower temperatures informed about a magnetic relaxation phenomenon (Fig. 1C). When measured at a frequency of 1 Hz, the out-of-phase susceptibility maximum temperature (T_{MAX}) of the pure *Drosophila* ferritin peaked at 6.4 ± 0.2 K. Elemental analysis using ICP-AES determined a concentration of 87.32 mg iron per g of the ferritin sample. Interestingly, the so determined zinc and manganese concentrations were 0.658 mg and 0.311 mg per g of sample, respectively; these values correspond to 6.4 atoms of zinc and 3.6 atoms of manganese per 1000 atoms of iron.

Magnetic characterization of whole fly samples suggests ferritins are more iron-loaded in mutants

Ferritin iron can be detected by the temperature dependence of the out-of-phase susceptibility.[18,19] Unambiguous signals could be obtained when the *Drosophila* genotypes were raised on diets supplemented with 1 mM FAC (Fig. 2).

The data from whole fly samples were compared with the data for pure ferritin. T_{MAX} was observed to depend on the fly genotype (Fig. 2). While the T_{MAX} of *Df(3R)Fer*/+ flies coincided with that of pure ferritin (6.9 ± 0.6 *vs.* 6.4 ± 0.2 K, respectively), the T_{MAX} of the *white* and *over* flies coincided at 4.3 ± 0.4 and 4.3 ± 0.6 K, respectively. A GFP-trap line in the *Fer1HCH* gene (encoded by the *Fer1HCH^{G188}* allele that inactivates one copy of

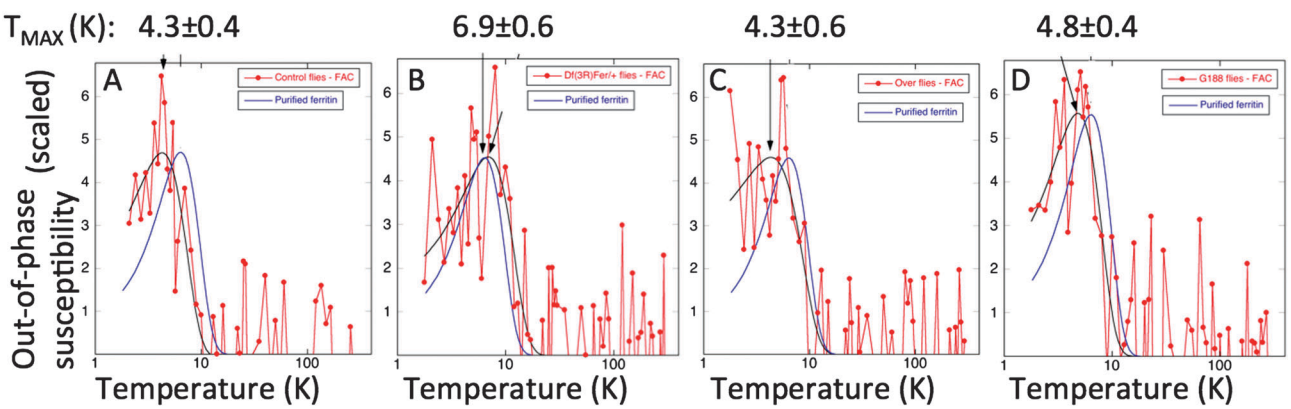

Fig. 2 Temperature dependence of the out-of-phase AC magnetic susceptibility of whole flies and pure ferritin. To facilitate the comparison, the vertical axis has been respectively scaled to get coincidence between the maxima of the fitting profiles (see Methods). The T_{MAX} calculated for the ferritin component in each sample is indicated at the top of each graph. All flies were grown on food supplemented with 1 mM FAC. Genotypes tested: (A) *white* (B) *Df(3R)Fer*/+ (C) *Actin-Gal4*/+; *UAS-Fer1HCH*, *UAS-Fer2LCH*/+ (D) *Fer1HCH^{G188}*/+.

the *Fer1HCH* gene) showed a T_{MAX} of 4.8 ± 0.4 K, an intermediate between the *white* controls and the *Df(3R)Fer*/+ heterozygous mutants, where one copy of *Fer1HCH* and *Fer2LCH* is deleted. Differences in T_{MAX} are normally indicative of related difference in the iron core size, or density or crystalline structure. To understand the structural basis for the observed differences in T_{MAX}, *Drosophila* ferritin was purified and observed under the transmission electron microscope (TEM).

3D reconstruction of *Drosophila* ferritin protein and iron cores using single particle imaging analysis

High resolution TEM was used to characterise the morphology of the holoferritin in *Drosophila* in both unstained and stained samples, respectively. Of the unstained iron core, a 4170 single particle data set was generated, and these single particles were iteratively refined by reference-free alignment[45] to build a three dimensional (3D) map based on 413 2D class averages with the widest range of angular orientations relative to one another (Fig. 3A). The quality of our unstained iron core 3D map is demonstrated by the overall agreement between comparing the 2D reprojections (Fig. 3B), derived from the final 3D map calculation, and the pre-map 2D class averages (Fig. 3A). The final 3D map was estimated by Fourier Shell Correlation[47] to have a resolution of 22 Å and revealed to be a roughly globular structure, but with well defined outer edges (Fig. 3C). The overall dimensions of the iron core ranged from a minimum of 70 Å to a maximum of 80 Å, again, in agreement with previously reported data for human liver ferritin.[54] Furthermore, variations in the internal density of the iron core manifested themselves within a region of low density at the centre of the molecular envelope, derived from all 2D averages merged, when a threshold at 2.5 σ (Fig. 3A and B) was applied. A range of diameters for this region of low density could be discerned upon closer inspection of individual 2D class averages from multi-variate statistical analysis (Fig. 4A), indicating a range of 3D models might be calculated with varying sizes of low density centres ranging from zero, *i.e.* no low density centre present, to 48 Å in diameter. Comparative studies on 20 341, in this case negatively stained holoferritin particles, resulted in 1874 2D class average projections with an inner core of similar dimensions and evidence of a central, low density space, as previously described for the unstained iron cores (Fig. 3D). These data were also used to construct a 3D map for the protein shell (Fig. 3F), giving a final estimated resolution of 24 Å (see Fig. S2, ESI†). Again, this 3D map was supported by the quality of the corresponding 2D reprojections (Fig. 3E) as back projections down through the same assigned Eulerian angles used to construct the final model. The 3D map of the protein shell was on average 120 Å in diameter and contains an inner cage, which satisfied a close visual fit to our 3D model of the unstained iron core (see overlaid 3D models revealing proportions between the protein shell (magenta) and iron core (green); Fig. 3G). Further support for our map was given by its striking compatibility with the crystallographic structure of *Trichoplusia ni* ferritin (Fig. 3H; pdb code 1Z6O).[28] The core contributed to roughly a quarter of the overall volume of the holoferritin (Fig. 3I). The central, low density space, as previously described for the unstained iron cores (Fig. 3A and B), was independently confirmed in the protein-stained samples (Fig. 3D). The low density space varied in size from being almost non detectable to 48 Å in diameter (Fig. 4A), a finding that remained robust after taking into account effects of Gaussian high pass filtering for a 3D reconstruction of ~80 Å in diameter. Thus, our structural studies were consistent with the view that iron loading of individual ferritin particles proceeds from the inner protein shell surface, with the iron core growing towards the central cavity, as shown previously for human liver ferritin.[54] The variation in size of the low-density

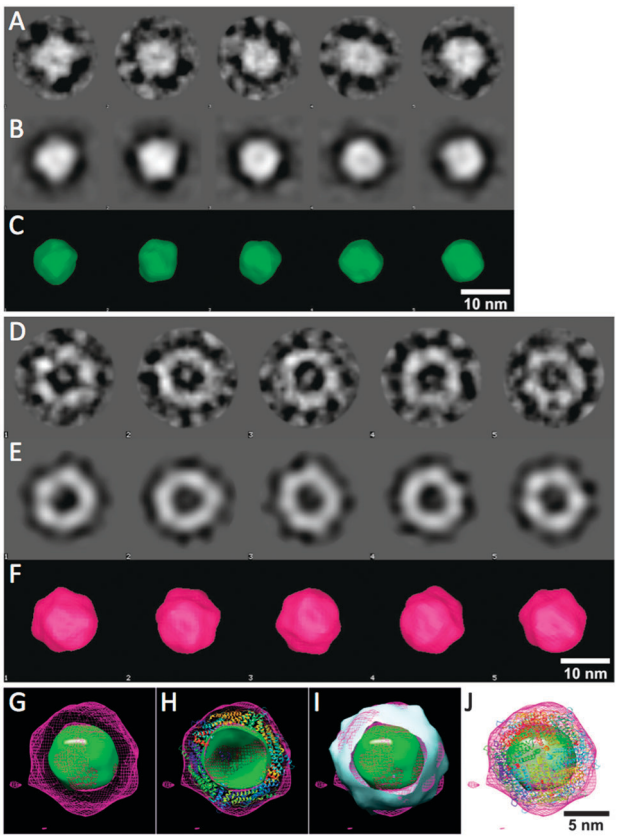

Fig. 3 Structural model of native *Drosophila* ferritin. Single particle image analyses on native *Drosophila* ferritin, resulting in the calculation of 3D maps for both holoferritin (coloured magenta) and iron core (coloured green), at approximately 24 Å resolution, as estimated by Fourier shell correlation (3 σ criterion). (A) Selection of five typical class averages used for the 3D reconstitution of unstained iron cores. (B) Reprojections from the 3D map in identical orientation as the class averages presented in A. (C) Surface-rendered views, in green, of the final 3D map viewed in these same orientations. Bar represents 10 nm. (D–F) As for A to C, but for stained holoferritin protein, in magenta. Bar represents 10 nm. (G–J) Molecular modelling environment whereby the ''fit to map'' function of the program UCSF Chimera[50] was used to fit the 3D map of the iron core (panel C, green) into that of the *Trichoplusia ni* ferritin structure co-ordinates 1Z6O.pdb (panel H, cross-sectional view, cartoon ribbons) and our TEM-derived holoferritin molecular envelope (panel J, magenta) with a correlation fit accuracy of 81.9% and 93.0% respectively. (I) The IZ6O.pdb co-ordinates were low-pass filtered to 24 Å resolution (white surface-rendered shell) and fit within the holoferritin (magenta), using the same Chimera ''fit to map'' function, with a correlation fit of 92.6%. (J) An alternative representation on a white background, no cross-section, holoferritin as magenta mesh, 1Z6O.pdb as cartoon ribbons, iron core as a green solid surface rendered view. Bar represents 5 nm.

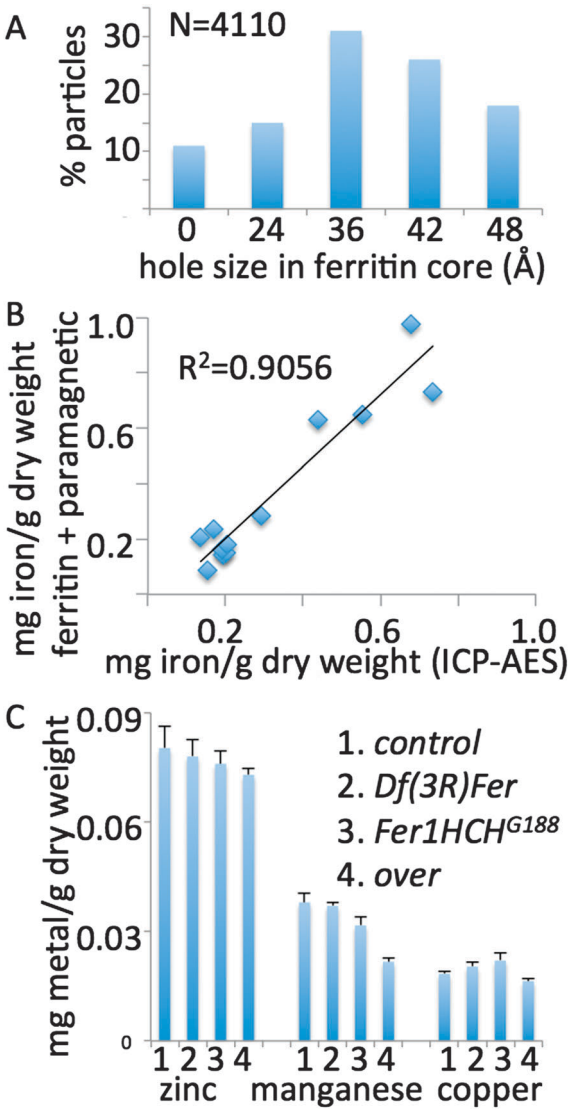

Fig. 4 (A) Histogrammatical representation for a 4110 two-dimensional projection data set of unstained ferritin cores (on carbon support), where the approximate diameter of an unstained sphere of low density, at a threshold of 2.5 σ, is shown against the % number of particles attributed to each sphere size. Zero Å relates to particles with no low density *i.e.* an apparently complete iron core; no iron cores were observed with an internal sphere of low density larger than 48 Å in diameter. (B) Linear regression of iron determination by ICP-AES and from the temperature dependence of AC magnetic susceptibility (ferritin iron is added to paramagnetic iron). Values are taken from Table 1. (C) Zinc, manganese and copper determination by ICP-AES in *white* control flies (1), *Df(3R)Fer*/+ heterozygous mutants (2), *Fer1HCH*^{G188}/+ heterozygous mutants (3) and *Actin-Gal4*/+; *UAS-Fer1HCH*, *UAS-Fer2LCH*/+ overexpression flies (4). *Over* flies accumulate half the manganese compared to the other three genotypes ($p < 0.001$, ANOVA).

core regions suggests that flies carried a distribution of ferritins differentially loaded with iron.

Flies overexpressing ferritin show a significant decrease in paramagnetic iron and manganese accumulation

The iron concentration in the ferritin and paramagnetic forms calculated from the magnetic measurements in the whole flies is shown in Table 1. Under normal diet, ferritin iron in *white* control flies was significantly higher than in *Df(3R)Fer*/+ heterozygous mutants, yet despite the marked difference, paramagnetic iron was very similar, suggesting iron homeostasis was operating successfully in the heterozygous flies. In contrast, flies overexpressing ferritin had a marked decrease in paramagnetic iron, suggesting that these flies were more significantly deprived of functional iron. Dietary iron supplementation increased the content of ferritin and paramagnetic iron in all genotypes, whereas iron chelation, using BPS in the diet had the opposite effect (Table 1). Ferritin iron accounted for most supplemented iron, consistent with previous observations,[20,22] yet the marked decrease in paramagnetic iron in *over* flies was consistent in all diets (Table 1).

Total iron was determined independently by ICP-AES (Table 1) and correlated well with the estimates produced by the magnetic analysis (Fig. 4B). *Df(3R)Fer*/+ heterozygous mutants showed reduced accumulation of total iron in all three diets and to a lesser extent this was also true for over flies, a finding that was observed independently by Tang and Zhou.[25] As the presence of iron in the diet seemed to have no influence on the accumulation of copper, zinc or manganese (Table 1)[53] the mean values for each metal per genotype were calculated using the different diets as independent replicates (Fig. 4C). *white* and *Df(3R)Fer*/+ flies accumulated 0.038 $\pm$ 0.003 and 0.037 $\pm$ 0.001 mg g^{-1} manganese, respectively, whereas flies that overexpress ferritin accumulated a significantly reduced amount of manganese, *i.e.* 0.022 $\pm$ 0.001 mg g^{-1}. Together with our observation that ferritin contained manganese our results implicate ferritin in the homeostasis of this metal. Genetic background controls are in progress to ensure that the decrease seen in manganese in the *Actin-Gal4*/+; *UAS-Fer1HCH*, *UAS-Fer2LCH*/+ overexpression flies can be specifically attributed to ferritin overexpression. Further tests are required to explore whether manganese binding to ferritin has a physiologic role, as results obtained here would suggest.

Discussion

Convergence of findings from magnetic analysis, electron microscopy, protein biochemistry and elemental analysis

A new structural model for *Drosophila* ferritin was generated (Fig. 3). The protein shell aligned closely with the *Trichoplusia ni* assembled ferritin crystal structure.[28] The overall diameter of the iron core was determined by the inner surface cavity of the protein shell (Fig. 3G) but reduced density was observed at the centre of the molecule (Fig. 3A, B and 4A) as reported for human hepatic ferritin.[54] Therefore, the observed differences in T_{MAX} seen in whole fly samples are most likely explained by differences in the iron loading of the cores. A T_{MAX} of 6.4 K for purified *Drosophila* ferritin (Fig. 1C) was slightly below the T_{MAX} values observed previously for mouse liver and serum ferritin (8 K and 10 K, respectively) and horse spleen ferritin (10 K).[55,56]

The *Fer1HCH*^{G188} allele adds GFP to the endogenous ferritin expressed from its normal chromosomal location.[20] This tool has served to observe changes in expression of ferritin caused by diverse dietary and genetic manipulations.[20,24,35,57,58]

As GFP-tagged ferritin loads with iron[20] it was unclear whether heterozygous *Fer1HCH*^{G188}/+ flies were in any way affected with regards to iron homeostasis. Ferritin iron in the *Fer1HCH*^{G188}/+ flies was reduced under normal dietary conditions (Table 1). The T_{MAX} of the AC out-of-phase magnetic susceptibility component was somewhat larger than controls (Fig. 2D). Therefore, heterozygous *Fer1HCH*^{G188}/+ flies showed a mild phenotype of reduced iron storage.

Total iron determination by ICP-AES strongly correlated with its determination using the magnetic properties of fly powder (Fig. 4B). Under normal diet, Prussian Blue staining of protein gels showed a decrease in ferritin iron in the heterozygous ferritin deficiency strain compared to control flies (Fig. 1A). The magnetic analysis also suggested that ferritin iron is halved in *Df(3R)Fer*/+ flies compared to control in normal diet (Table 1). Under iron supplementation, this difference in ferritin iron loading was no longer seen in protein gels (Fig. 1A) or in magnetic measurements (Table 1). Therefore findings from classic biochemical analysis were in agreement with those of the magnetic analysis. The iron cores of ferritin from *Df(3R)Fer*/+ showed a higher T_{MAX} value compared to ferritin from control flies in AC out-of-phase magnetic susceptibility measurements (Fig. 2A and B). Hence, the fewer ferritins that accumulated in the *Df(3R)Fer* heterozygous mutant compared to the control flies had a greater iron loading. In other words, total ferritin iron was similar between the two genotypes in these conditions but their ferritins were differentially loaded.

Ferritin overexpression results in functional iron deficiency

The notion that ferritin overexpression results in functional iron deficiency is not new[17,20] and has been proposed as an explanation for the neurodegenerative phenotype of mice that also overexpress ferritin due to a lack of iron regulatory proteins.[59,60] To our knowledge our results provide the first direct demonstration that bioavailability of iron decreased in flies that overexpress ferritin (see paramagnetic iron measurements in Table 1). This result supports the view that the protective effects of neuronal ferritin overexpression in *Drosophila* models of disease are related to iron sequestration in neurons.[30–33] It is also relevant for studies relating ferritin and iron to insect-host interactions.[61–63] More perplexing was the finding that the T_{MAX} of the *white* and *over* flies coincided at 4.3 K, suggesting that some assembled ferritin in the *over* flies is likely iron-poor. One possible interpretation of this finding is that cells may differ in their ability to load iron to ferritin.[24,35]

Evidence for a role of ferritin in the homeostasis of zinc and manganese

No storage protein is known at present for manganese. Assuming that each ferritin molecule contained on average over 1000 atoms of iron, three or more atoms of manganese and six or more atoms of zinc were bound per ferritin molecule. Therefore, it is conceivable that ferritin could also serve as a reservoir for manganese and zinc. Flies overexpressing ferritin accumulated markedly less iron and manganese but were no different in total zinc content (Fig. 4C). We believe the reductions in iron and manganese in *over* flies can be explained by ferritin excretion in the gut lumen.[23] It is known that very low levels of labile zinc are found in cells under normal conditions.[64] Zinc might therefore not be readily available to overexpressed ferritin. Nevertheless, the situation could be very different under conditions of zinc overload, as in the case in the posterior intestine following dietary zinc supplementation.[35] Dietary zinc induces ferritin in an MTF-1-dependent manner,[34,35] but it was previously unclear what purpose was served as such ferritin did not accumulate iron.[35] Ferritin in the posterior midgut could directly bind excess zinc and therefore function in conditions of zinc overload to sequester this metal ion. Therefore, our findings, taken together with previous observations in the literature,[34–38] implicate ferritin in zinc and manganese homeostasis.

Conclusions

Purified *Drosophila* ferritin contained a few atoms of manganese and zinc. Together with other genetic evidence we propose ferritin is directly involved in the homeostasis of these metals, likely serving as a metal sink. Magnetic characterization of the isolated ferritin enabled the measurement of iron partitioning in whole fly samples. Cell and tissue homeostasis can cope with reduced levels of ferritin expression, but overexpression of ferritin leads to functional iron deficiency. Temperature-dependent AC magnetic susceptibility can be used to determine iron partitioning between ferritin and other proteins in complex biological samples.

Acknowledgements

J.N. held a Royal Society University Research Fellowship for the majority of this work. L.G. holds a Sara Borrell postdoctoral contract (CD09/00030) from the ISCIII-MSPS. We thank Dr Norbert Krauss (Queen Mary, University of London) for shared use of laboratory equipment and critical review of the manuscript, Dr Robin Maytum (University of Bedfordshire) for early discussions and technical advice, Prof. Hermann Steller (Rockefeller University) as the *Df(3R)Fer* chromosome was engineered in his laboratory. This work was supported by the CONACYT project 179835 to F.M.

References

1 E. C. Theil, *Curr. Opin. Chem. Biol.*, 2011, **15**, 304–311.
2 P. Arosio, R. Ingrassia and P. Cavadini, *Biochim. Biophys. Acta*, 2009, **1790**, 589–599.
3 S. C. Andrews, *Biochim. Biophys. Acta*, 2010, **1800**, 691–705.
4 D. Q. Pham and J. J. Winzerling, *Biochim. Biophys. Acta*, 2010, **1800**, 824–833.
5 S. Hasegawa, S. Saito, J. Takanashi, Y. Morokoshi, T. Furukawa, T. Saga and I. Aoki, *Magn. Reson. Imaging*, 2011, **29**, 179–184.
6 B. Iordanova and E. T. Ahrens, *NeuroImage*, 2012, **59**, 1004–1012.

7 H. S. Kim, H. J. Joo, J. S. Woo, Y. S. Choi, S. H. Choi, H. Kim and W. K. Moon, *Mol. Imaging Biol.*, 2012, **15**, 48–57.
8 G. V. Velde, *et al.*, *NeuroImage*, 2012, **62**, 367–380.
9 S. Lee, K. H. Lee, J. S. Ha, S. G. Lee and T. K. Kim, *Angew. Chem., Int. Ed.*, 2011, **50**, 8709–8713.
10 K. Li, Z. P. Zhang, M. Luo, X. Yu, Y. Han, H. P. Wei, Z. Q. Cui and X. E. Zhang, *Nanoscale*, 2012, **4**, 188–193.
11 J. B. Delehanty and I. L. Medintz, *ChemBioChem*, 2012, **13**, 30–33.
12 K. Fan, C. Cao, Y. Pan, D. Lu, D. Yang, J. Feng, L. Song, M. Liang and X. Yan, *Nat. Nanotechnol.*, 2012, **7**, 459–464.
13 D. Kaur, F. Yantiri, S. Rajagopalan, J. Kumar, J. Q. Mo, R. Boonplueang, V. Viswanath, R. Jacobs, L. Yang, M. F. Beal, D. DiMonte, I. Volitaskis, L. Ellerby, R. A. Cherny, A. I. Bush and J. K. Andersen, *Neuron*, 2003, **37**, 899–909.
14 P. O. Berberat, M. Katori, E. Kaczmarek, D. Anselmo, C. Lassman, B. Ke, X. Shen, R. W. Busuttil, K. Yamashita, E. Csizmadia, S. Tyagi, L. E. Otterbein, S. Brouard, E. Tobiasch, F. H. Bach, J. W. Kupiec-Weglinski and M. P. Soares, *FASEB J.*, **17**, 1724–1726.
15 D. Kaur, S. Rajagopalan and J. K. Andersen, *Brain Res.*, 2009, **1297**, 17–22.
16 S. Hasegawa, Y. Morokoshi, H. Kanda, S. Tsukamoto, J. Zheng, A. B. Tsuji, T. Furukawa, S. Kakinuma, Y. Shimada and T. Saga, *Carcinogenesis*, 2012, **33**, 2269–2275.
17 J. th. Wilkinson, X. Di, K. Schonig, J. L. Buss, N. D. Kock, J. M. Cline, T. L. Saunders, H. Bujard, S. V. Torti and F. M. Torti, *Biochem. J.*, 2006, **395**, 501–507.
18 L. Gutierrez, M. V. Spasic, M. U. Muckenthaler and F. J. Lazaro, *Biochim. Biophys. Acta*, 2012, **1822**, 1147–1153.
19 M. Whitnall, Y. S. Rahmanto, M. L. Huang, F. Saletta, H. C. Lok, L. Gutierrez, F. J. Lazaro, A. J. Fleming, T. G. St Pierre, M. R. Mikhael, P. Ponka and D. R. Richardson, *Proc. Natl. Acad. Sci. U. S. A.*, 2012, **109**, 20590–20595.
20 F. Missirlis, S. Kosmidis, T. Brody, M. Mavrakis, S. Holmberg, W. F. Odenwald, E. M. Skoulakis and T. A. Rouault, *Genetics*, 2007, **177**, 89–100.
21 S. Kosmidis, J. A. Botella, K. Mandilaras, S. Schneuwly, E. M. Skoulakis, T. A. Rouault and F. Missirlis, *Neurobiol. Dis.*, 2011, **43**, 213–219.
22 F. Missirlis, S. Holmberg, T. Georgieva, B. C. Dunkov, T. A. Rouault and J. H. Law, *Proc. Natl. Acad. Sci. U. S. A.*, 2006, **103**, 5893–5898.
23 M. Locke M and H. Leung, *Tissue Cell*, 1984, **16**, 739–766.
24 A. Mehta, A. Deshpande, L. Bettedi and F. Missirlis, *Biochimie*, 2009, **91**, 1331–1334.
25 X. Tang and B. Zhou, *FASEB J.*, 2012, **27**, 288–298.
26 A. Charlesworth, T. Georgieva, I. Gospodov, J. H. Law, B. C. Dunkov, N. Ralcheva, C. Barillas-Mury, K. Ralchev and F. C. Kafatos, *Eur. J. Biochem.*, 1997, **247**, 470–475.
27 T. Georgieva, B. C. Dunkov, S. Dimov, K. Ralchev and J. H. Law, *Insect Biochem. Mol. Biol.*, 2002, **32**, 295–302.
28 A. E. Hamburger, A. P. West, Jr., Z. A. Hamburger, P. Hamburger and P. J. Bjorkman, *J. Mol. Biol.*, 2005, **349**, 558–569.
29 S. Li, *Cell Res.*, 2010, **20**, 1148–1157.
30 C. S. Mendes, C. Levet, G. Chatelain, P. Dourlen, A. Fouillet, M. L. Dichtel-Danjoy, A. Gambis, H. D. Ryoo, H. Steller and B. Mollereau, *EMBO J.*, 2009, **28**, 1296–1307.
31 T. Rival, R. M. Page, D. S. Chandraratna, T. J. Sendall, E. Ryder, B. Liu, H. Lewis, T. Rosahl, R. Hider, L. M. Camargo, M. S. Shearman, D. C. Crowther and D. A. Lomas, *Eur. J. Neurosci.*, 2009, **29**, 1335–1347.
32 Z. Wu, Y. Du, H. Xue, Y. Wu and B. Zhou, *Neurobiol. Aging*, 2012, **33**, 199.e1–199.e12.
33 G. Esposito, M. Vos, S. Vilain, J. Swerts, J. de Sousa Valadas, S. van Meensel, O. Schaap and P. Verstreken, *PLOS Genet.*, 2013, **9**, e1003478.
34 H. Yepiskoposyan, D. Egli, T. Fergestad, A. Selvaraj, C. Treiber, G. Multhaup, O. Georgiev and W. Schaffner, *Nucleic Acids Res.*, 2006, **34**, 4866–4877.
35 L. Gutierrez, N. Sabaratnam, R. Aktar, L. Bettedi, K. Mandilaras and F. Missirlis, *FEBS Lett.*, **584**, 2942–2946.
36 M. Sadraie and F. Missirlis, *Biometals*, 2011, **24**, 679–686.
37 D. Price and J. G. Joshi, *Proc. Natl. Acad. Sci. U. S. A.*, 1982, **79**, 3116–3119.
38 P. De Sole, C. Rossi, M. Chiarpotto, G. Ciasca, B. Bocca, A. Alimonti, A. Bizzarro, C. Rossi and C. Masullo, *Clin. Biochem.*, 2013, **46**, 89–93.
39 S. Pead, E. Durrant, B. Webb, C. Larsen, D. Heaton, J. Johnson and G. D. Watt, *J. Inorg. Biochem.*, 1995, **59**, 15–27.
40 F. C. Meldrum, T. Douglas, S. Levi, P. Arosio and S. Mann, *J. Inorg. Biochem.*, 1995, **58**, 59–68.
41 B. Zhang, J. N. Harb, R. C. Davis, J. W. Kim, S. H. Chu, S. Choi, T. Miller and G. D. Watt, *Inorg. Chem.*, 2005, **44**, 3738–3745.
42 T. Rakshit and R. Mukhopadhyay, *Langmuir*, 2011, **27**, 9681–9686.
43 B. C. Dunkov, D. Zhang, K. Choumarov, J. J. Winzerling and J. H. Law, *Arch. Insect Biochem. Physiol.*, 1995, **29**, 293–307.
44 G. Tang, L. Peng, P. R. Baldwin, D. S. Mann, W. Jiang, I. Rees and S. J. Ludtke, *J. Struct. Biol.*, 2007, **157**, 38–46.
45 M. van Heel, G. Harauz, E. V. Orlova, R. Schmidt and M. Schatz, *J. Struct. Biol.*, 1996, **116**, 17–24.
46 P. Dube, P. Tavares, R. Lurz and M. van Heel, *EMBO J.*, **12**, 1303–1309.
47 M. van Heel, *Ultramicroscopy*, 1987, **21**, 111–123.
48 M. Radermacher, *J. Electron Micros. Tech.*, 1988, **9**, 359–394.
49 M. van Heel and M. Schatz, *J. Struct. Biol.*, 2005, **151**, 250–262.
50 E. F. Pettersen, T. D. Goddard, C. C. Huang, G. S. Couch, D. M. Greenblatt, E. C. Meng and T. E. Ferrin, *J. Comput. Chem.*, 2004, **25**, 1605–1612.
51 J. García Palacios, *Adv. Chem. Phys.*, 2000, **112**, 1–210.
52 B. C. Dunkov and T. Georgieva, *DNA Cell Biol.*, 1999, **18**, 937–944.
53 L. Bettedi, M. F. Aslam, J. Szular, K. Mandilaras and F. Missirlis, *J. Exp. Biol.*, 2011, **214**, 971–978.
54 Y. H. Pan, K. Sader, J. J. Powell, A. Bleloch, M. Gass, J. Trinick, A. Warley, A. Li, R. Brydson and A. Brown, *J. Struct. Biol.*, 2009, **166**, 22–31.
55 L. A. Cohen, L. Gutierrez, A. Weiss, Y. Leichtmann-Bardoogo, D. L. Zhang, D. R. Crooks, R. Sougrat, A. Morgenstern,

B. Galy, M. W. Hentze, F. J. Lazaro, T. A. Rouault and E. G. Meyron-Holtz, *Blood*, 2010, **116**, 1574–1584.
56 F. Luis, E. Del Barco, J. M. Hernández, E. Remiro, J. Bartolomé and J. Tejada, *Phys. Rev. B: Condens. Matter Mater. Phys.*, 1999, **59**, 11837–11846.
57 A. Mehta, A. Deshpande and F. Missirlis, *Biochem. Soc. Trans.*, 2008, **36**, 1313–1316.
58 H. Uhrigshardt, T. A. Rouault and F. Missirlis, *J. Biol. Inorg. Chem.*, 2013, **18**, 441–449.
59 S. S. Cooperman, E. G. Meyron-Holtz, H. Olivierre-Wilson, M. C. Ghosh, J. P. McConnell and T. A. Rouault, *Blood*, 2005, **106**, 1084–1091.
60 M. C. Ghosh, W. H. Tong, D. Zhang, H. Ollivierre-Wilson, A. Singh, M. C. Krishna, J. B. Mitchell and T. A. Rouault, *Proc. Natl. Acad. Sci. U. S. A.*, 2008, **105**, 12028–12033.
61 G. Chamilos, R. E. Lewis, J. Hu, L. Xiao, T. Zal, M. Gilliet, G. Halder and D. P. Kontoyiannis, *Proc. Natl. Acad. Sci. U. S. A.*, 2008, **105**, 9367–9372.
62 N. Kremer, D. Voronin, D. Charif, P. Mavingui, B. Mollereau and F. Vavre, *PLoS Pathog.*, 2009, **5**, e1000630.
63 K. Mandilaras, T. Pathmanathan and F. Missirlis, *Nutrients*, 2013, **5**, 1622–1647.
64 W. Maret, *Adv. Nutr.*, 2013, **4**, 82–91.